

Sheaf Neural Networks and biomedical applications

A. Merhab*, J.-W. Van Looy*, P. Demurtas*,
S. Iotti*, E. Malucelli*, F. Rossi*, F. Zanchetta*, R. Fioresi*
* University of Ferrara, Italy; * University of Bologna, Italy

Abstract. The purpose of this paper is to elucidate the theory and mathematical modelling behind the sheaf neural network (SNN) algorithm and then show how SNN can effectively answer to biomedical questions in a concrete case study and outperform the most popular graph neural networks (GNNs) as graph convolutional networks (GCNs), graph attention networks (GAT) and GraphSage.

1 Introduction

Graph Neural Networks (GNNs) [27] provide an effective framework for learning from relational data that may be represented as a graph, hence they are especially fruitful when treating real and challenging datasets of biomedical significance. Sheaf Neural Networks (SNNs) are a relatively new family of Deep Learning (DL) algorithms, generalizing Graph Neural Networks (GNNs), obtained by equipping graphs with an extra algebraic structure [5, 2], namely a *sheaf structure*, which brings along a new enhanced version of the message passing mechanism and a more fruitful aggregation of node features.

The purpose of this work is to show how SNNs can be effectively used in a concrete case study, involving a biomedical dataset, and outperform the most popular graph neural networks in a biologically significant classification task. This dataset consists of spectroscopic measurements from patients affected by osteosarcoma, a highly aggressive primary bone tumor, characterized by abnormal bone mineralization processes [23, 24]. Understanding the biochemical alterations in bone tissues, associated with tumor development is therefore crucial for improving diagnosis and prognosis. The dataset is obtained via synchrotron-based X-ray absorption spectroscopy, and details bone tissue chemical composition at micro and nanoscopic scales, providing information on chemical and structural changes associated with disease progression [25]. To better capture the relationships between samples beyond

individual spectral features, we represent the dataset as a graph, where each node corresponds to a tissue sample and edges are defined by cosine similarity in the reduced spectral space after principal component analysis (PCA). Each node is then associated with features, providing information on tissue properties and it is labelled as tumor/no tumor for the binary classification task we will perform. This graph-based representation provides a natural framework for sheaf neural networks, with their enhanced representation and classification capabilities.

Our work is organized as follows.

In Sec. 2 we briefly recap the concept of sheaf on a graph and we compare the definitions appearing in the literature e.g. cellular sheaves [6], with a focus on the neural network applications [5] introducing also the Laplacian operator as instrumental to the message passing mechanism.

In Sec. 3 we present the biomedical dataset, and its graph realization, together with its biological significance. Then describe our sheaf neural network (SNN) model, together with the GCN, GAT and GraphSage models and the training procedure we followed (see also the App. A for more details).

In Sec. 4 we present the performance of the SNN model benchmarked against the most successful GNN models described previously.

In Sec. 5 we present the conclusions and we suggest future applications of SNNs to biomedical dataset analysis including clustering and many graph settings.

2 Sheaves on Graphs

In this section we recap the theory of sheaves on graphs, focusing on the graph neural network applications (see [9] and refs. therein for the full bibliography). We first give the usual notion of sheaf on a topological space and then we relate it to the notion of *cellular sheaf* as it is the one used for the machine learning applications. Most of this material is well known, however the treatment of directed/undirected graphs as preordered sets or topological spaces, deserves some attention, since in the SNN treatments [5, 2] the definitions regarding sheaves on graphs are not the mainstream ones.

2.1 Sheaves

The concept of sheaf, introduced by Leray in [18] (see also [13]), is central in geometry and captures the essence of the geometrical object it is describing: topological manifolds, differentiable manifolds or algebraic schemes to cite a few key examples. Such mathematical objects are defined locally, but exhibit global behavior which are governed by suitable compatibility conditions. The concept of sheaf provides a framework for describing how local data on these objects can be assembled to describe global data on them in a coherent way. For completeness, we briefly recap the key definitions (see [7, 17] for a quick introduction to all notions needed here).

Definition 2.1. Let X be a topological space. A *presheaf* \mathcal{F} on X is an assignment $U \mapsto \mathcal{F}(U)$, where U open in X and $\mathcal{F}(U)$ is a set, and for each inclusion of open sets $V \subseteq U$, we have a *restriction map*

$$\rho_V^U : \mathcal{F}(U) \rightarrow \mathcal{F}(V),$$

satisfying $\rho_U^U = \text{id}$ and $\rho_W^V \circ \rho_V^U = \rho_W^U$ whenever $W \subseteq V \subseteq U$. We say \mathcal{F} is a sheaf of groups (rings, vector spaces etc.), if $\mathcal{F}(U)$ is a group (ring, vector space etc.).

Let $U \subseteq X$ be an open set and $\{U_i\}_{i \in I}$ an open cover of U . A presheaf \mathcal{F} is called a *sheaf* if it satisfies the following:

1. *Locality.* If $s, t \in \mathcal{F}(U)$ satisfy $s|_{U_i} = t|_{U_i}$ for all $i \in I$, then $s = t$.
2. *Gluing.* If for each $i \in I$ there exists a section $s_i \in \mathcal{F}(U_i)$ such that $s_i|_{U_i \cap U_j} = s_j|_{U_i \cap U_j}$ for all $i, j \in I$, then there exists a unique section $s \in \mathcal{F}(U)$ with $s|_{U_i} = s_i$ for all $i \in I$.

Example 2.2. The Sheaf of Differentiable Functions. Let M be a differentiable manifold [17]. For each open set $U \subseteq M$, define

$$\mathcal{C}^\infty(U) = \{f : U \rightarrow \mathbb{R} \mid f \text{ is smooth}\}.$$

If $V \subseteq U$, the restriction map sends a smooth function $f \in \mathcal{C}^\infty(U)$ to its restriction $f|_V \in \mathcal{C}^\infty(V)$. This assignment defines a presheaf of rings on M , which is in fact a sheaf. Smooth functions defined on an open cover on M can be glued together to produce a unique smooth function on M , [17].

Observation 2.3. Given a base \mathcal{B} for the topology on X , a \mathcal{B} -sheaf \mathcal{F} on X is an assignment $U \mapsto \mathcal{F}(U)$, for all $U \in \mathcal{B}$ satisfying the definition of sheaf when restricted to the open sets in \mathcal{B} , with suitable modifications (see [7] Ch. I). We have that any \mathcal{B} -sheaf on X extends uniquely to a sheaf on X (Prop. I-12 in [7]).

We now focus on graphs. Let $G = (V, E)$ be a (undirected) graph, V the set of its vertices, E its edges. We can define a preorder \leq on G as follows.¹ Let x, y be vertices or edges of G . We say $x \leq y$ if $x = y$ or x is a vertex of the edge y . As for any finite set with a preorder, we can define a topology by giving a base for the open sets as follows:

$$U_p := \{q \in G \mid p \leq q\} \quad p \in G$$

where, with an abuse of notation, we see G as the union of its vertices and edges.

This topology is called the *Alexandrov topology* [16, 1]. We notice that U_p are *irreducible*, that is there is no smaller open set containing p and strictly contained in U_p . Irreducible open sets represent an important difference with the continuous setting, where such open sets do not exist.

As one can readily check:

- $U_v = \{e \in E \mid v \leq e\} \cup \{v\}$, that is the open star of v , for each vertex $v \in V$,
- $U_e = \{e\}$, i.e. the edge e , without its vertices, for each $e \in E$.

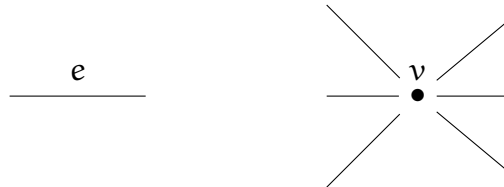


Figure 1: Irreducible open sets for the Alexandrov topology on graphs

¹A preorder differs from an order by not requiring that $x \leq y, y \leq x$ implies $x = y$.

Observation 2.4. 1. A sheaf F of vector spaces on a graph G viewed as a topological space as above, is determined by a \mathcal{B} -sheaf F on the irreducible open sets. Such F consists of:

- an assignment of a vector space $F(\mathbf{U}_v)$ for each vertex $v \in V_G$.
- an assignment of a vector space $F(\mathbf{U}_e)$ for each edge $e \in E_G$.
- an assignment of linear maps (restriction maps) $F_{v \leq e} : F(\mathbf{U}_v) \rightarrow F(\mathbf{U}_e)$ for each $v \leq e$ (we have $\mathbf{U}_e \subset \mathbf{U}_v$ whenever $v \leq e$).

We leave to the reader the easy check that this assignment gives indeed a \mathcal{B} -sheaf.

2. This notion of sheaves on graphs, as described in (1), is the same as the one introduced by Bodnar et al. in [5, 6, 12] in the context of *cellular sheaves*, which are defined directly on preordered sets associated with regular cell complexes. Indeed, if we specialize the definition of cellular sheaf to the special case of a graph, viewed as a regular cellular cell complex, by definition we have that a cellular sheaf F is an assignment: $x \rightarrow F(x)$, $F(x)$ a vector space, for each cell vertex or edge x . Moreover if $v \leq e$, i.e. if v is a vertex of the edge e we have a linear map $F_{v \leq e} : F(\mathbf{U}_v) \rightarrow F(\mathbf{U}_e)$. Thus we recover a sheaf, via the remarks in 1., in the usual sense i.e. as in Def. 2.1.

2.2 Sheaf Laplacian

We define the sheaf Laplacian operator and then we compare it to the GNN message passing mechanism.

For every presheaf of vector spaces \mathcal{F} on a graph $G = (V, E)$ we define 1 and 0 chains as follows:

$$C_1(G, \mathcal{F}) := \bigoplus_{e \in E} \mathcal{F}(e), \quad C_0(G, \mathcal{F}) := \bigoplus_{v \in V} \mathcal{F}(v)$$

where to ease the notation we use $\mathcal{F}(x)$ in place of $\mathcal{F}(\mathbf{U}_x)$, for x a vertex or an edge.

For a given orientation on G , we define the coboundary operator

$$\delta : C_0(G, \mathcal{F}) \rightarrow C_1(G, \mathcal{F})$$

by

$$(\delta x)_e := F_{u \leq e}(x_u) - F_{v \leq e}(x_v),$$

$x = \{x_v \in \mathcal{F}(v)\}_{v \in V} \in C_0(\mathbf{G}, \mathcal{F})$, $\delta x \in C_1(\mathbf{G}, \mathcal{F})$ and e is the edge connecting u and v .

We may view δ as a generalization of the incidence matrix of \mathbf{G} , that is, we see δ as an operator from the function on vertices to the functions on edges of the graph (see [26] for more details).

The *sheaf Laplacian* is defined as

$$\mathcal{L}_{\mathcal{F}} = \delta^\top \delta : C_0(\mathbf{G}, \mathcal{F}) \longrightarrow C_0(\mathbf{G}, \mathcal{F}),$$

This is a positive semi-definite operator acting on $C_0(\mathbf{G}, \mathcal{F})$, and its kernel can be identified with the global sections of the sheaf \mathcal{F} .

When $\mathcal{F}(v) = \mathbb{R}$, for all v , and all restriction maps are identities, that is the case when \mathcal{F} equals to the constant sheaf \mathbb{R} on \mathbf{G} , $\mathcal{L}_{\mathcal{F}}$ reduces to the standard graph Laplacian $L = D - A$ [26], where D is the degree matrix and A the adjacency matrix of \mathbf{G} [26].

2.3 GNN message passing mechanisms

In order to understand how sheaf Laplacians can improve the design of GNNs, we need to say more about how GNNs and SNNs are implemented in applications. To this end, we need to introduce a few notions. To start with, a *graph \mathbf{G} with features h_v* consists of the datum of a graph \mathbf{G} together with a vector of features $h_v \in \mathbb{R}^n$ for each node v of it. We shall write such datum as $(\mathbf{G}, h_{\mathbf{G}})$ where $\mathcal{F} : V_{\mathbf{G}} \rightarrow \mathbb{R}^n$, $h_{\mathbf{G}}(v) := h_v$.

A typical GNNs and CNNs layer will modify the feature vector from step i to step $i + 1$ as follows:

$$h_v^{(i+1)} = \sigma_i(\psi_i(\text{GConv}_i(\mathbf{G}, h_{\mathbf{G}}^{(i)})_v) + \alpha_i h_v^{(i)} W_i) \quad (1)$$

where:

- σ_i is an activation function (see [4]), that is a multivariate ridge functions.
- GConv_i is a *graph convolution*, i.e. an operator that updates the vector of features according to a so called *message passing* mechanism (see [4], [10]). This is where the key difference between GNNs and SNNs occurs.
- ψ_i is usually a regularizing function, $\alpha_i \in \mathbb{R}$ and W_i is a $n_i \times n_{i+1}$ matrix of weights (this is known also as a *skip-connection* mechanism, see [4]).

A simple example of a graph convolution to use in Eq. 1, is the one where each GConv_i updates the node features using the ordinary graph Laplacian, that is

$$\text{GConv}(\mathbf{G}, \mathbf{h}_G^{(i)})_{\mathbf{v}} = - \sum_{\mathbf{u} \in \mathcal{N}(\mathbf{v})} \mathbf{h}_u^{(i)} \mathbf{W}^{(i)} + \mathbf{d}(\mathbf{v}) \mathbf{h}_v^{(i)} \mathbf{W}^{(i)}$$

where $\mathcal{N}(\mathbf{v})$ denotes the set of nodes connected with an edge to \mathbf{v} , $\mathbf{d}(\mathbf{v}) = |\mathcal{N}(\mathbf{v})|$ the degree of \mathbf{v} and $\mathbf{W}^{(i)}$ is a $\mathbf{n}_i \times \mathbf{n}_{i+1}$ matrix of weights. Fixed an ordering on the nodes of \mathbf{G} , if we denote as $\mathbf{H}^{(i)} \in \mathbb{R}^{|\mathbf{V}_G| \times \mathbf{n}_i}$ the matrix having as rows the vectors $\mathbf{h}_v^{(i)}$, $\mathbf{v} \in \mathbf{V}_G$, this convolution can be written in the following compact form, that is often found in literature.

$$\text{GConv}_i(\mathbf{G}, \mathbf{h}_G^{(i)}) = \mathbf{A} \mathbf{H}^{(i)} \mathbf{W}^{(i)}$$

where \mathbf{A} is the adjacency matrix of \mathbf{G} . Many of the most popular graph convolutions used in GNNs are a modified version of this one. A GNN employing such convolutions can be thought as a discretizing an heat equation diffusing the information stored in each vector of features along the edges at each layer, see [4, 10].

We can see the datum of a graph with features $(\mathbf{G}, \mathbf{h}_G)$ as the datum of a graph \mathbf{G} together with \mathbf{n} sections of the constant sheaf $\underline{\mathbb{R}}^{\mathbf{n}} \cong \bigoplus_{i=1}^{\mathbf{n}} \underline{\mathbb{R}}$. Convolutions as the one just described for the the i th layer of a GNN can then be interpreted as operators $\mathbf{C}_0(\mathbf{G}, \underline{\mathbb{R}})^{\mathbf{n}_i} \rightarrow \mathbf{C}_0(\mathbf{G}, \underline{\mathbb{R}})^{\mathbf{n}_{i+1}}$ that, using a terminology familiar to the readers working in deep learning, transform sections of the constant sheaf $\underline{\mathbb{R}}$ on \mathbf{G} having \mathbf{n}_i channels to sections of the constant sheaf $\underline{\mathbb{R}}$ on \mathbf{G} having \mathbf{n}_{i+1} channels using a mechanism based on the application of $\mathbf{L}_{\underline{\mathbb{R}}}$.

The idea of diffusing the information of the node features along the edges of \mathbf{G} can be then reinterpreted as the idea of diffusing the information along the stalks of a constant sheaf (see [5, 12]). This idea can then be generalized to the case when we deal with non-constant sheaves, giving rise to the so called sheaf neural networks (see [5] for an explanation and more references).

In SNNs the convolutional layer as in (1) is then replaced by:

$$\mathbf{h}_v^{(i+1)} = \sigma_i(((\Delta_{\mathcal{F}^{(i)}}(\mathbf{I} \otimes \mathbf{W}_1^{(i)}) \mathbf{h}_G^{(i)})_{\mathbf{v}} \mathbf{W}_2^{(i)} + \alpha_i \mathbf{h}_v^{(i)} \mathbf{W}_3^{(i)})) \quad (2)$$

where:

- σ_i is an activation function.

- $\Delta_{\mathcal{F}^{(i)}}$ is the sheaf Laplacian $\mathcal{L}_{\mathcal{F}^{(i)}}$ or the *normalised* sheaf Laplacian $D_{\mathcal{F}^{(i)}}^{-1/2} \mathcal{L}_{\mathcal{F}^{(i)}} D_{\mathcal{F}^{(i)}}^{-1/2}$ (see [5, 12]) where, after the identification of $\mathcal{L}_{\mathcal{F}^{(i)}}$ with a $(\mathbf{d} \times \mathbf{f}_i) \times (\mathbf{d} \times \mathbf{f}_i)$ matrix, $D_{\mathcal{F}^{(i)}}$ is the block diagonal of $L_{\mathcal{F}^{(i)}}$.
- $W_1^{(i)}$, $W_2^{(i)}$ and $W_3^{(i)}$ are a $\mathbf{d} \times \mathbf{d}$, a $\mathbf{f}_i \times \mathbf{f}_{i+1}$ and a $\mathbf{f}_i \times \mathbf{f}_{i+1}$ matrices of weights respectively.
- \otimes denotes the Kronecker product.
- $\alpha_i \in \mathbb{R}$.

Explicitly note that in the case $\mathcal{F}^{(i)} = \underline{\mathbb{R}}$ for all i , Eq.2 coincide with Eq.1 where ψ_i is the identity and GConv_i are the simple Laplacian-based convolutions we described before. SNN are then more flexible than ordinary Laplacian-based GNN as, modeling sheaves that can have a deeper structure than $\underline{\mathbb{R}}$, allow message passing mechanisms that do not treat all the edge relations to be equal allowing the resulting networks to learn complex interactions between nodes that are deeper than the ones contained in an adjacency matrix or in a weighted adjacency matrix (see [5] for a discussion).

3 Sheaf and Graph Neural Networks

In this section we want to illustrate with a concrete case study the advantage of the sheaf Laplacian message passing mechanism with respect to the standard ones, as illustrated in the previous section. We will first briefly introduce the biological dataset and the classification question we want to solve. Then, we compare the performance of some sheaf neural network models and we benchmark them against popular graph neural network algorithms as GCN, GraphSage, GAT ([15, 11, 29]).

3.1 The biomedical question

The dataset we examine is obtained from a series of spectroscopic measurements, regarding both healthy and tumor bone tissues, of osteosarcoma patients. Osteosarcoma [23, 25] is a highly aggressive primary bone tumor and it is linked to abnormal mineralization processes in the bones. The dataset is obtained via synchrotron-based X-ray absorption near edge structure (XANES) spectroscopy and describes bone tissue chemical composition

at micro- and nanoscopic scales, providing detailed information on chemical and structural changes associated with disease progression. Advanced spectroscopic methods, such as synchrotron-based X-ray spectroscopy [3, 22] and infrared (IR) spectroscopy [28, 19], can be used to provide detailed information on chemical structure. In particular, synchrotron-based XANES spectroscopy is an X-ray absorption spectroscopy technique that provides insights into the oxidation state and local coordination geometry of specific chemical elements constituting the analyzed sample. In the context of osteosarcoma disease, the chemical environment of calcium is of paramount interest as this element is a constituent of the mineral fraction of bone tissue. To obtain the dataset, XANES spectra were collected from 224 points of interest at a pixel size of $1 \times 1 \mu\text{m}^2$ with the incident beam energy being varied between 4.02 keV and 4.17 keV at 0.3 eV steps across the Ca-K edge (see [25] for more details of the experimental procedure followed to obtain data). This resulted in a dataset of 224 XANES spectra, each one consisting of 501 data points. Each of the 224 samples was labeled as 1 (tumor) or 0 (control), depending on whether the tissue was tumoral or healthy. This produced a labeled dataset with 147 tumor samples and 77 control samples. To this data we assigned the structure of graph with features as follows. First, we perform PCA on the data to reduce the dimension of the spectra to 50 (in our case, this still accounts for almost 100% of the variance of the dataset). In the case we consider a train/valid/test split on the samples, PCA is fitted only on the training spectra, and the resulting dimensionality-reduction model is then applied to all samples. Then, we construct a graph with features $\mathbf{G}_{\text{bio}} = (\mathbf{G}_{\text{pca}}, \mathbf{h}_{\mathbf{G}_{\text{pca}}})$, where each node \mathbf{v} corresponds to a sample and its feature vector $(\mathbf{h}_{\mathbf{G}_{\text{pca}}})_{\mathbf{v}} \in \mathbb{R}^{50}$ is the 50-dimensional PCA representation of its spectrum. To create the edges, we compute the cosine similarity between every pair of nodes and sort these values from highest to lowest. Edges are then added following this order, starting from the pairs with the highest cosine similarity, until the graph becomes connected. Given this graph, our goal is to train an algorithm that, taking \mathbf{G}_{bio} as input, predicts the label of each node, that is, whether each sample, representing a node, is tumoral or control.

3.2 Our GNN and SNN models

We first describe the 3 types of GNN model we tested to benchmark our SNN and then we go to describe the latter in detail. Each of GNN models employs

layers following Eq. 1 and they differ just for the type of graph convolutions. The GCN, SAGE and GAT convolution are found in [15, 11, 29]. We now describe these models in detail.

GCN. This is a GNN consisting of q layers following Eq. 1 where:

- GConv_i , for all $i = 1, \dots, q$ is as in [15].
- if $i \neq q$, ψ_l a normalization function, W_i is equal to the identity matrix if $n_l = n_{l+1}$ and $\alpha_l = 1$. ψ_q is the identity function and $\alpha_q = 0$.
- σ_l the ReLU activation function [4] ($i \neq q$) and σ_q is the identity function.

In addition, dropout [4] is applied after each layer.

GraphSAGE. This is a GNN consisting of q layers following Eq. 1 where:

- GConv_i , for all $i = 1, \dots, q$ is the GraphSage convolution [11], that we implemented using the relative function found in PyG [8] (and setting the hyperparameter `normalize` to be equal to `True`)
- if $i \neq q$, ψ_l a normalization function, W_i is equal to the identity matrix if $n_l = n_{l+1}$ and $\alpha_l = 0.05$. ψ_q is the identity function and $\alpha_q = 0$.
- σ_l the ReLU activation function ($i \neq q$) and σ_q is the identity function.

In addition, dropout is applied after each layer.

GAT. This is a GNN consisting of q layers following Eq. 1 where:

- GConv_i , for all $i = 1, \dots, q$ is the GAT convolution [29], that we implemented using the relative function found in PyG [8] (and setting the hyperparameter `normalize` to be equal to `True`)
- if $i \neq q$, ψ_l a normalization function, W_i is equal to the identity matrix if $n_l = n_{l+1}$ and $\alpha_l = 1$. ψ_q is the identity function and $\alpha_q = 0$.
- σ_l the ELU activation function [4] ($i \neq q$) and σ_q is the identity function.

In addition, dropout is applied after each layer. We will detail the hyperparameters of the specific models we tested in Appendix A. For all the GNNs we implemented, we have used as regularization function a combination of batch and layer normalization using the functions `torch_geometric.nn.BatchNorm` and `torch.nn.LayerNorm` of PyG [8] and Pytorch [20] respectively.

Sheaf diffusion models. The SNN model we tried consist of a SNN having layers following Eq. 2. Note that in our experiments the sheaf of each layer is *learned*, as in [5], and the sheaves involved at each layer have general, unconstrained restriction maps. In addition, we used the normalized graph Laplacian, we used the same number of channels in each layer and we set $W_3^{(i)}$ as in Eq. 2 to be equal to the identity matrix if $n_l = n_{l+1}$. We denote this model as SheafGeneral.

4 Experiments and results

We trained the models described in Section 3.2 as node (binary) classifiers, i.e. as models that given as an input the graph with features as described in Section 3.1, return a label 0 or 1 for each node.

We trained our models in a transductive setting ([4]). Recall that under transductive training, for a given train/valid/test split of the nodes, the model receives the full graph topology and all node features, including those of test nodes, but only the labels of the training nodes. Because our dataset contains only 224 samples, we evaluated our algorithms using a 10-fold stratified cross-validation (CV [4]), combined with a grid search over the hyperparameters of each of the six models we considered. In a 10-fold stratified CV, the dataset is partitioned into ten equally sized, non-overlapping subsets that preserve the original class distribution, resulting in ten distinct train/test splits (the folds). Within each fold, we further split the training portion into an 90/10 train/validation set: PCA is then fit on each reduced training fold set and used to determine the edges G_{pca} for the given fold. For each hyperparameter configuration in the grid, the corresponding model is trained on the fold’s training set and evaluated on both the validation and test sets. This entire procedure is repeated 5 times, each time starting from a different random shuffle of the dataset. For each model type, we then select the best hyperparameter configuration based on the mean validation accuracy across the 5 repetitions of the ten-fold cross-validation. Details on the hyperparameter spaces are provided in Appendix A. A summary of the work-

Model	Fold Accuracy (mean \pm std)	Majority Vote Acc (95% CI)
SheafGeneral	0.9779 \pm 0.033	0.9866 (0.961–0.995)
GraphSAGE	0.9187 \pm 0.061	0.9286 (0.887–0.956)
GAT	0.7719 \pm 0.080	0.7812 (0.723–0.830)
GCN	0.7603 \pm 0.075	0.7634 (0.704–0.814)

Table 1: Performances of the models on our dataset.

flow is shown in Fig. 2. Table 1 reports two metrics for each model type. The first, Fold Accuracy, is the mean test-set accuracy across the five repetitions of the ten-fold cross-validation, where in each fold the model was trained on the train fold set using the best hyperparameters during grid search as explained before. The second metric is the Majority Vote Accuracy. Since each node appears in exactly one test fold and the cross-validation is repeated 5 times, each model type produces 5 potentially different label predictions for every node. A final label is then assigned to each node by taking the majority vote over these predictions. Using these majority-vote labels, we compute the Majority Vote Accuracy, reported together with its confidence interval in Table 1. This metric offers a complementary perspective on model performance. It is worth noting that neither our evaluation metrics nor the overall structure of our experimental design are intended to assess the out of sample performance of a final deployed model or to identify the most generalizable solution to the task. Instead, our goal is to compare the architectures under consideration and determine which of them exhibits the greatest expressive power for the problem at hand.

Our models were written using the PyTorch library [20] in the Python environment. For training our models, we used the Adam optimizer [14] with a learning rate scheduler. The details of the implementation can be found in Appendix A.

Our experiments found that SheafGeneral was the model that achieved the best performance, surpassing the performance of all the other models. We also notice that GraphSage was the only vanilla GNN model achieving a performance comparable to the one of the SNNs we tested.

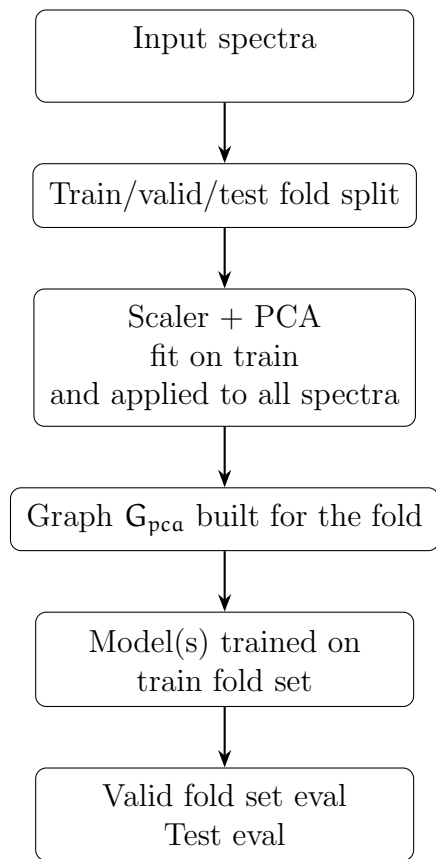


Figure 2: Training and evaluation workflow for each cross-validation iteration.

5 Conclusions

We have provided a mathematical introduction to Sheaf Neural Networks showing how they generalize ordinary Laplacian-based graph neural networks. We then showed how SNNs enhanced generalization capabilities can effectively answer in a concrete biomedical case study to relevant biologically grounded questions, outperforming popular graph neural networks. Future studies will be directed to analyze datasets consisting of many graphs and enhancing furtherly the SNN capability towards clustering algorithms and their biomedical applications.

6 Acknowledgements

This research was supported by Gnsaga-Indam, by COST Action CaLISTA CA21109, HORIZON-MSCA-2022-SE CaLIGOLA, MSCA-DN CaLiForNIA - 101119552, PNRR MNESYS, PNRR National Center for HPC, Big Data and Quantum Computing, PNRR SymQuSec and INFN Sezione Bologna.

7 Contribution

F. Zanchetta, R. Fioresi contributed in writing the paper and conceptual design of the research questions. A. Merhab, J.-W. Van Looy, P. Demurtas contributed in writing both the paper and the code. S. Iotti, E. Malucelli, F. Rossi contributed with the biological problem and dataset.

References

- [1] F.G. Arenas. Alexandroff spaces. *Acta Mathematica Universitatis Comenianae. New Series*, 68(1):17–25, 1999.
- [2] Federico Barbero, Cristian Bodnar, Haitz Sáez de Ocáriz Borde, Michael Bronstein, Petar Veličković, and Pietro Liò. Sheaf neural networks with connection laplacians. In *Topological, Algebraic and Geometric Learning Workshops 2022*, pages 28–36, 2022.
- [3] Paul M Bertsch and Douglas B Hunter. Applications of synchrotron-based x-ray microprobes. *Chemical Reviews*, 101(6):1809–1842, 2001.
- [4] Christopher M. Bishop and Hugh Bishop. *Deep Learning - Foundations and Concepts*. Springer, New York, 2024.
- [5] Cristian Bodnar, Francesco Di Giovanni, Benjamin Paul Chamberlain, Pietro Lio’, and Michael M. Bronstein. Neural sheaf diffusion: A topological perspective on heterophily and oversmoothing in gnns. *ArXiv*, abs/2202.04579, 2022.
- [6] Justin Michael Curry. *Sheaves, cosheaves and applications*. 2014.
- [7] David Eisenbud and Joe Harris. *The Geometry of Schemes*, volume 197 of *Graduate Texts in Mathematics*. Springer, New York, 2000.

- [8] Matthias Fey and Jan Eric Lenssen. Fast graph representation learning with pytorch geometric. *CoRR*, abs/1903.02428, 2019.
- [9] Rita Fioresi, Angelica Simonetti, and Ferdinando Zanchetta. Sheaves on graphs and their differential calculi. *preprint*, 2026.
- [10] Rita Fioresi and Ferdinando Zanchetta. Deep learning and geometric deep learning: an introduction for mathematicians and physicists. *International Journal of Geometric Methods in Modern Physics*, 20(12):2330006, 2023.
- [11] William L. Hamilton, Zhitao Ying, and Jure Leskovec. Inductive representation learning on large graphs. In Isabelle Guyon, Ulrike von Luxburg, Samy Bengio, Hanna M. Wallach, Rob Fergus, S. V. N. Vishwanathan, and Roman Garnett, editors, *Advances in Neural Information Processing Systems 30: Annual Conference on Neural Information Processing Systems 2017, December 4-9, 2017, Long Beach, CA, USA*, pages 1024–1034, 2017.
- [12] Jakob Hansen and Robert Ghrist. Toward a spectral theory of cellular sheaves. *Journal of Applied and Computational Topology*, 3(4):315–358, 2019.
- [13] Christian Houzel. *A Short History: Les débuts de la théorie des faisceaux*, pages 7–22. Springer Berlin Heidelberg, Berlin, Heidelberg, 1990.
- [14] Diederik P. Kingma and Jimmy Ba. Adam: A method for stochastic optimization. In Yoshua Bengio and Yann LeCun, editors, *3rd International Conference on Learning Representations, ICLR 2015, San Diego, CA, USA, May 7-9, 2015, Conference Track Proceedings*, 2015.
- [15] Thomas N. Kipf and Max Welling. Semi-supervised classification with graph convolutional networks. In *5th International Conference on Learning Representations, ICLR 2017, Toulon, France, April 24-26, 2017, Conference Track Proceedings*, 2017. OpenReview.net.
- [16] Czes Kosniowski. *A First Course in Algebraic Topology*. Cambridge Mathematical Textbooks. Cambridge University Press, Cambridge, 1980.

- [17] John M. Lee. *Introduction to Smooth Manifolds*, volume 218 of *Graduate Texts in Mathematics*. Springer, New York, 2012.
- [18] Jean Leray. L’anneau d’homologie d’une représentation. *Comptes rendus hebdomadaires des séances de l’Académie des sciences*, 222:1366–1368, 1946.
- [19] Lily M Ng and Reiko Simmons. Infrared spectroscopy. *Analytical chemistry*, 71(12):343–350, 1999.
- [20] Adam Paszke, Sam Gross, Francisco Massa, Adam Lerer, James Bradbury, Gregory Chanan, Trevor Killeen, Zeming Lin, Natalia Gimelshein, Luca Antiga, Alban Desmaison, Andreas Köpf, Edward Z. Yang, Zachary DeVito, Martin Raison, Alykhan Tejani, Sasank Chilamkurthy, Benoit Steiner, Lu Fang, Junjie Bai, and Soumith Chintala. Pytorch: An imperative style, high-performance deep learning library. In Hanna M. Wallach, Hugo Larochelle, Alina Beygelzimer, Florence d’Alché-Buc, Emily B. Fox, and Roman Garnett, editors, *Advances in Neural Information Processing Systems 32: Annual Conference on Neural Information Processing Systems 2019, NeurIPS 2019, December 8-14, 2019, Vancouver, BC, Canada*, pages 8024–8035, 2019.
- [21] F. Pedregosa, G. Varoquaux, A. Gramfort, V. Michel, B. Thirion, O. Grisel, M. Blondel, P. Prettenhofer, R. Weiss, V. Dubourg, J. Vanderplas, A. Passos, D. Cournapeau, M. Brucher, M. Perrot, and E. Duchesnay. Scikit-learn: Machine learning in Python. *Journal of Machine Learning Research*, 12:2825–2830, 2011.
- [22] F Peyrin. Investigation of bone with synchrotron radiation imaging: from micro to nano. *Osteoporosis international*, 20(6):1057–1063, 2009.
- [23] Jörg Ritter and SS Bielack. Osteosarcoma. *Annals of oncology*, 21:vii320–vii325, 2010.
- [24] Paschalis Roschger, EP Paschalis, P Fratzl, and K Klaushofer. Bone mineralization density distribution in health and disease. *Bone*, 42(3):456–466, 2008.
- [25] Francesca Rossi, Giovanna Picone, Concettina Cappadone, Andrea Sorrentino, Marta Columbaro, Giovanna Farruggia, Emilio Catelli, Giorgia

- Sciutto, Silvia Prati, Robert Oliete, et al. Shedding light on osteosarcoma cell differentiation: Impact on biomineralization and mitochondria morphology. *International Journal of Molecular Sciences*, 24(10):8559, 2023.
- [26] Gordon F Royle and Chris Godsil. *Algebraic graph theory*, volume 207. Springer, New York, 2001.
- [27] Franco Scarselli, Marco Gori, Ah Chung Tsoi, Markus Hagenbuchner, and Gabriele Monfardini. The graph neural network model. *IEEE transactions on neural networks*, 20(1):61–80, 2008.
- [28] Barbara Stuart. Infrared spectroscopy. *Kirk-Othmer encyclopedia of chemical technology*, 2000.
- [29] Petar Velickovic, Guillem Cucurull, Arantxa Casanova, Adriana Romero, Pietro Liò, and Yoshua Bengio. Graph attention networks. In *6th International Conference on Learning Representations, ICLR 2018, Vancouver, BC, Canada, April 30 - May 3, 2018, Conference Track Proceedings*, 2018.

A Supplementary material

A.1 Implementation details

GCN (and setting the parameter `normalize` to be equal to `True`) We report in Table 2 the precision, recall, F1-score, and AUC (Area Under the Curve, see [4]) achieved the best models tested, computed using the same methodology adopted for the Majority Vote Accuracy in Section 4. The hyperparameter spaces explored in our grid searches are listed in Tables 4, 3, 5, 6, and the best hyperparameter configurations identified are shown in Table 7. For each hyperparameter space, all the grid searches performed have been exhaustive. These configurations were used to train the models whose results appear in Tables 2 and 1. We used the built-in Adam optimizer provided by PyTorch, together with the `ReduceLROnPlateau` scheduler from the same library; hyperparameters not included in the grid search were kept at their default values. All trainings were run for 400 epochs, and we did not subdivide the training nodes into batches. For GNN models, early stopping with patience

is used. PCA and cosine similarity were computed using the built-in functions of Scikit-learn [21]. For the graph convolutions employed in our GNNs, we used the implementations available in PyTorch Geometric [8], while the SNN was implemented from scratch in PyTorch. We shall now list all the abbreviations found in the tables below:

- `hidden_dim` refers to the feature dimension of each layer (the n_i in Eq. 1 if $i \neq 1, q + 1$).
- `num_layers` is the number of identical layers of the GNN or the SNN considered.
- `dropout` is the dropout rate applied after each layer.
- `lr` is the learning rate.
- `weight_decay` is the weight decay parameter of the Adam optimizer.
- `patience` is the patience parameter set to stop training.
- `sched_patience` is the patience parameter given to the scheduler.
- `min_epochs` is the minimum number of training epochs before patience can be applied.
- `grad_clip` is the parameter applied to clip the gradients.
- `heads` is the number of heads. This parameter is specific to GAT layers. In this case Constraint: `hidden_dim` must be divisible by `heads` in the configuration tested.
- The hyperparameters `f` and `d` of the SheafGeneral are the sheaf dimensions and the number of channels as in Eq- 2.

A.2 Dataset origin

Three osteosarcoma patients were chosen for the study, and their bone specimens were collected during elective surgery at Istituto Ortopedico Rizzoli (IOR) (Bologna, Italy) prior Ethical Committee approval (744/2019/Sper/IOR) with written informed consent obtained from each patient.

Model	Vote Prec.	Vote Rec.	Vote F1	Vote AUC
SheafGeneral	1.0000	0.9796	0.9897	0.9969
GraphSAGE	0.9712	0.9184	0.9441	0.9483
GAT	0.7753	0.9388	0.8492	0.7616
GCN	0.7611	0.9320	0.8379	0.6850

Table 2: Additional metrics for the final experiment.

GraphSAGE hyperparameter	values
hidden_dim	{16, 32, 64}
num_layers	{2, 3, 4}
dropout	{0.1, 0.2, 0.3}
lr	{0.001, 0.002, 0.005, 0.01, 0.05}
weight_decay	{1e-5, 1e-4, 2e-4}

Table 3: GraphSAGE grid search. Total configurations: 405.

GCN hyperparameter	values
hidden_dim	{32, 64, 128}
num_layers	{2, 3, 4}
dropout	{0.1, 0.2, 0.3}
lr	{0.002, 0.005, 0.01, 0.05, 0.2, 0.5}
weight_decay	{1e-5, 1e-4}
patience	{80}
min_epochs	{200}
sched_patience	{40}
grad_clip	{1.0, 2.0, 3.0}

Table 4: GCN grid search. Total configurations: 972.

GAT hyperparameter	values
hidden_dim	{32, 64, 128}
num_layers	{2, 3, 4}
dropout	{0.1, 0.2, 0.3}
lr	{0.001, 0.002, 0.005, 0.01, 0.05, 0.2, 0.5}
weight_decay	{1e-5, 1e-4}
patience	{80}
min_epochs	{200}
sched_patience	{40}
grad_clip	{2.0}
heads	{2, 4}

Table 5: GAT grid search space. Total configurations: 756.

SheafGeneral hyperparameter	values
d	{4, 6, 8}
f	{12, 16, 24}
num_layers	{2, 4}
dropout	{0.1, 0.2, 0.3}
lr	{0.05, 0.1, 0.2, 0.25}
weight_decay	{1e-3, 1e-4}
activation	ELU
patience	100
grad_clip	{1.0}

Table 6: Sheaf grid search space focused on general sheaves. Total configurations: 432.

Model	hyperparameters
SheafGeneral	type=general, d=8, f=24, L=2, act=ELU, drop=0.2, lr=0.01, wd= 10^{-3} , $\gamma=0.5$, pat=50, clip=0.5
GraphSAGE	h=32, L=2, drop=0.1, lr=0.005, wd= 10^{-4} , pat=80, min_ep=100, sched_pat=40, ls=0.1, clip=2
GAT	h=32, L=4, heads=2, drop=0.1, lr=0.002, wd= 10^{-5} , pat=80, min_ep=200, sched_pat=40, clip=2
GCN	h=32, L=3, drop=0.2, lr=0.002, wd= 10^{-5} , pat=80, min_ep=200, sched_pat=40, clip=1

Table 7: Best hyperparameter configurations found with our grid search for each model type.